Composites: Part A 198 (2025) 109131

Contents lists available at ScienceDirect

Composites Part A

journal homepage: www.elsevier.com/locate/compositesa

Degradation mechanisms of CF/PPS, CF/PEI, and CF/PEEK under combined UV radiation and condensation

Annelise Jean-Fulcrand [a], Ewen Léger [a], Frédéric Dau [b,c], Martine Dubé [a], Ilyass Tabiai [a,*]

[a] CREPEC, Department of Mechanical Engineering École de Technologie Supérieure, 1100, rue Notre-Dame Ouest, Montréal, H3C 1K3, Québec, Canada
[b] FLYING WHALES, 13-17 rue Pages, Suresnes, F-92150, France
[c] ENSAM/Lab. I2M UMR CNRS, 5395, Espalnades des Arts et Métiers, Talence, F-33405, France

GRAPHICAL ABSTRACT

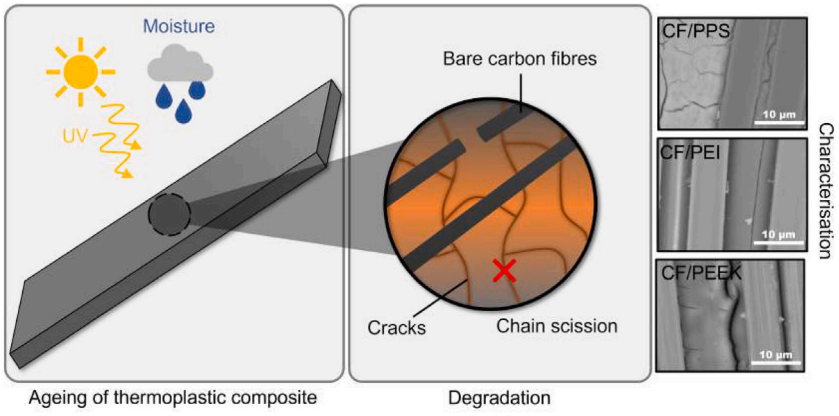

ARTICLE INFO

Keywords:
Carbon fibre-reinforced thermoplastic composite
Accelerated degradation
Mechanical performance

ABSTRACT

From 1990 to 2020, the total weight of composites integrated in airplane structures increased from 5 to 50% contributing to reduce fuel consumption and CO_2 emission. However, environmental weathering conditions alter the stability and durability of load-bearing composite components. Three carbon fibre-reinforced high-performance thermoplastic composites — polyphenylene sulphide (PPS), polyether imide (PEI), and polyether ether ketone (PEEK) — used in aviation are exposed to combined ultraviolet radiation (UV), humidity and temperature, following ASTM D4329-21 for up to 28 days. To support characterisation, the corresponding neat polymer films of PPS, PEI, and PEEK were aged under the same conditions. The polymer matrix of the composites degraded following two distinct mechanisms. CF/PPS predominantly cross-linked, which resulted in increased brittleness, reduced crystallinity and increased in tensile strength after 28 days. In contrast, CF/PEI and CF/PEEK underwent primarily chain scission, leading to decreased T_g (PEI), increased crystallinity (PEEK), and reduced tensile strength (CF/PEEK and CF/PEI) after exposure.

* Corresponding author.
E-mail address: ilyass.tabiai@etsmtl.ca (I. Tabiai).

https://doi.org/10.1016/j.compositesa.2025.109131
Received 19 February 2025; Received in revised form 16 June 2025; Accepted 17 June 2025
Available online 30 June 2025

1. Introduction

The application of carbon fibre-reinforced polymer composites in the aviation and aerospace fields has experienced significant growth, now constituting approximately 50% of the total weight of aircraft structures. This tendency is motivated by rising fuel prices and the imperative to reduce CO_2 emissions, necessitating the use of lightweight, durable, and high-strength materials [1]. In a composite, the polymeric matrix also called resin, can be categorised as either thermoset or thermoplastic [2].

While thermosetting resins, particularly epoxy, have historically dominated composite applications, there is a growing interest in thermoplastic resin systems [3]. Initially, thermoplastics such as polyamide and polycarbonate [4] were perceived as lacking in mechanical and thermal properties [3]. Over the years, their properties were enhanced by optimising the polymer's molecular structure. The incorporation of rigid aromatic rings to strengthen intermolecular forces and flexible groups such as sulphide (polyphenylene sulphide), sulfone (polyethersulfone), ester (polyethylene terephthalate), and ether (polyetherimide) led to the development of high-performance thermoplastics [5] that exhibit superior thermomechanical properties and can sustain extensive damage without failure. As the performance of thermoplastics becomes comparable to thermosetting materials, their use as substitutes for thermosets increases, driven by their superior mouldability, recyclability, and lower cost of production [5,6]. Despite their numerous advantages, thermoplastics have limitations, such as their high processing temperatures and melt viscosity, which complicate their processing and make it challenging to achieve proper fibre impregnation. Additionally, their sensitivity to the surrounding environment with UV radiation and humidity often leading to premature material degradation and failure [7]. While considerable research has been dedicated to improving the properties of composites, as well as their shaping and assembly, their durability under weathering conditions remains underexplored [8]. Major concerns relate to the performance of the composite after long-term exposure to environmental weathering like UV radiation and water absorption [8,9]. Water absorption can lead to reversible degradation in the form of plasticisation or irreversible chemical ageing such as hydrolysis, oxidation, chain scission, and cross-linking [10,11].

Due to the popularity of carbon fibre-reinforced epoxy composites - a thermoset matrix polymer - in the aviation industry, the effects of various weathering conditions and UV radiation on their degradation have been widely studied [12,13]. A significant detrimental effect on the longevity of carbon fibre-reinforced epoxy is its hygroscopicity, which can rapidly lead to structural failure of the polymer matrix [11]. At the opposite, the limited use of carbon fibre-reinforced thermoplastics in such applications results in limited research and substantial knowledge gaps in this area. Out of all the thermoplastics, the superior temperature resistance of polyether ether ketone (PEEK) and its derivatives, relative to other high-performance thermoplastics such as polyphenylene sulphide (PPS) and polyether imide (PEI), establishes them as the preferred matrix materials for carbon fibre-reinforced composite components in aerospace and aviation applications, despite their significantly higher cost [14,15]. Because of the widespread usage of poly(aryl ether)-based composites in the industry, the research on their degradation linked to extreme weathering conditions such as UV radiation, temperature, and humidity is the most extensive [16–19]. Unfortunately, the majority of degradation studies on thermoplastics have primarily concentrated on the polymer itself, rather than its behaviour within a composite [20]. Among the few studies on fibre-reinforced thermoplastic composites exposed to extreme weathering conditions, Niu et al. [21] investigated the combined effect of UV radiation and water condensation on the degradation of carbon fibre-reinforced PEEK (CF/PEEK), while Dolo et al. [17] focused on its thermal exposure. Batista et al. [22,23] studied the impact of different degrees of crystallinity on CF/PEEK and carbon fibre-reinforced polyphenylene sulphide (CF/PPS) degradation under combined UV radiation and condensation, hygrothermal, and salt fog exposure. The impact of different weathering conditions on the mechanical and thermal performance of CF/PPS composites was also evaluated [7,24,25]. Several studies assessed the effect of hygrothermal ageing on glass fibre-reinforced PEI [26] and PPS [9]. However, these studies used different ageing methodologies (e.g. water immersion versus condensation, UV powers, temperatures) to assess the degradation of high-performance thermoplastic composites, making it difficult to conduct a reliable comparative analysis.

In this study, the combined effects of UV-A radiation and water condensation on three high-strength, lightweight carbon fibre-reinforced thermoplastic composites are examined. This research offers a comparative analysis of carbon fibre-reinforced PPS, PEI, and PEEK composites, focusing on the impact of prolonged environmental ageing on their properties. A range of analytical techniques is employed to characterise the materials, including tensile testing to assess mechanical strength, scanning electron and confocal microscopy to investigate morphological changes, energy dispersive X-ray spectroscopy and Fourier-transform infrared spectroscopy (FTIR) for chemical analysis, and differential scanning calorimetry (DSC) to evaluate thermal properties.

2. Materials and methods

2.1. Materials and specimen preparation

Three different carbon fibre-reinforced thermoplastic samples supplied by Toray Advanced Composites (Netherlands) were manufactured to achieve a final laminate thickness of 2.5 mm. Per the supplier's guidelines, all plies used to produce the laminates were dried overnight at 120 °C. The material properties of all thermoplastic composites are detailed in Table 1. Carbon fibre/polyether imide (CF/PEI) laminates were fabricated using unidirectional pre-impregnated Toray Cetex® TC1000 Design plies, containing a 66/34 carbon fibre to resin ratio by weight. These laminates were produced via compression moulding of CF/PEI pre-impregnated plies to create balanced $[0,90]_{4s}$ composite laminates. They were heated to 350 °C (recommended processing temperature T_p) under a pressure of 0.3 MPa for 15 min. Following this, the pressure was raised to 2 MPa for another 15 min to consolidate the laminate before gradually cooling to room temperature over approximately 60 min. Throughout the cooling phase, pressure was maintained. Similarly, the CF/PPS laminates were fashioned using unidirectional pre-impregnated Toray Cetex® TC1100 Design plies with the same weight fraction of carbon fibre to resin and a $[0,90]_{3s}$ configuration. The plies were heated to 315 °C and consolidated under 1 MPa for 15 min before cooling while maintaining pressure. Finally, CF/PEEK laminates in a $[0,90]_{4s}$ configuration, were prepared using Toray Cetex® TC1200 Design plies. These plies were heated to 380 °C with a pressure of 1 MPa and consolidated under 2 MPa pressure for 20 min, followed by cooling under pressure. CF laminates were used for various analyses, including optical photography, confocal microscopy, and scanning electron microscopy to investigate surface wear and topography, as well as energy-dispersive X-ray spectroscopy for chemical composition analysis, and mechanical testing. Additional pure polymer films, composed of the same resin and supplied by Toray with a thickness of 80 μm, were also subjected to ageing in the environmental chamber. These films were included to facilitate chemical (infrared spectroscopy) and thermal characterisation (differential scanning calorimetry).

Table 1
Materials properties of the different thermoplastic composites.

Materials	Thermal			Mechanical	Type	CF/resin
	T_g °C	T_m °C	T_p °C	tensile strength 0° MPa		mass ratio
CF/PEI Toray Cetex TC1000	217	N/A	350	516	Amorphous	66\34
CF/PPS Toray Cetex TC1100	90	280	315	736	Semi-crystalline	66\34
CF/PEEK Toray Cetex TC1200	143	343	380	776	Semi-crystalline	66\34

2.2. Ageing conditioning

Before ageing, to simulate the detrimental effects of UV radiation coupled with water condensation, all thermoplastic composite specimens measuring 250 × 25 × 2.5 mm^3 for mechanical testing as well as smaller pre-cut samples for other type of characterisations were placed within a weathering chamber and subjected to various exposure durations: 3, 10, 21, and 28 days, equivalent to total radiation doses of 230, 770, 1620 and 2150 kJ/m^2, respectively. All samples were pre-conditioned before ageing, following ASTM G147-17 [27]. The degradation mechanisms were assessed in accordance with ASTM D4329-21 [28], which outlines the methodology for testing in a UV radiation weathering chamber (QUV Accelerated Weathering Tester; Q-Panel Lab Products, USA). The cycle exposure consisted of 8-h intervals under UV-A light at 60 °C and 4-h intervals under water condensation at 50 °C. The UV-A radiation was generated using fluorescent UV lamps emitting wavelengths at 340 nm with an irradiance of 0.89 W/m^2.

2.3. Characterisation

2.3.1. Mechanical characterisation

The tensile mechanical properties of unaged and aged coupons were conducted on universal testing machine (MTS Alliance RF/200) with a 200 kN load cell and with an axial extensometer (MTS, 634.25) according to ASTM D3039/D3039M-17 [29], with a crosshead displacement speed of 2 mm/min. Tensile testing of cross-ply carbon fibre reinforced polymers laminates was chosen over other methods [30] to evaluate overall mechanical performance and reveal how UV-induced damage impacts load transfer and structural integrity, offering a comprehensive assessment of ageing effects. The specimens were cut into coupons of 250 × 25 × 2.5 mm^3 according to the standard. Glass fibre-reinforcement tabs (56 × 15 × 1.5 mm^3) were glued with HysolEA9696-modified polyurethane adhesive and cured at 110 °C for 90 min on both ends of the coupons. Four coupons were tested in each group, and the tensile strength and modulus obtained were calculated according to ASTM D3039/D3039M-17 [29]. The elastic modulus (E) was calculated using the chord modulus method, from ASTM D3039/D3039M-17 [29]. Specifically, E was determined by calculating the slope of the stress–strain curve between 0.1% and 0.3% strain.

2.3.2. Wear and surface characterisations

Samples were cut from a larger plate using a Diamond band saw BS200 S prior to the ageing process. They were rinsed with deionised (DI) water, dried with paper towels, and pre-conditioned in accordance with ASTM G147-17 [27]. Each sample was exposed for a specified duration and was not reused or reprocessed for further ageing. All samples originated from a single batch. The morphologies of the unaged and aged composites were examined using the BackScattered Electron (BSE) mode of a Scanning Electron Microscope (SEM) at 15 kV energy (Hitachi TM3000, Hitachi High-Technologies, Japan) and at a magnification of 6000× to highlight the crack formation and surface morphology of the samples. Before SEM analysis, the samples were dried in an oven set at 120 °C overnight. The photographs were taken using a Canon DS126231 camera and a SIGMA 105 mm 1:2:8 DG Macro HSM lens. The pristine and aged surfaces of the composite samples were observed with confocal microscopy (OLS 4100, LEXT, Olympus) at a magnification of 1000x and with an x,y resolution of 0.12 μm and a depth resolution of 10 nm. Three areas for each sample are measured. To quantify the extent of polymer removal from the surface, 28 line profiles were extracted for each sample to measure the arithmetic average roughness (Ra) and the average maximum penetration depth. To calculate the average maximum penetration depth, the minimum value from each surface profile, corresponding to the deepest point of polymer removal, was recorded. This method offers a localised and targeted measurement of material loss, in contrast to Ra, which provides a more general assessment of the overall surface texture.

2.3.3. Thermal characterisation

Thermal evaluation of the polymer films before and after exposure was carried out using a differential scanning calorimeter (DSC2500, TA Instruments, USA). Measurements were performed on the pure polymer rather than the CF composite due to the low signal intensity from the high CF content. While this approach ensures reliable data for the polymer phase, CF may influence crystallinity [30]. PPS and PEI samples were heated once up to 350 °C, and to 400 °C for PEEK at a sweep rate of 10 °C/min in an inert nitrogen atmosphere. Next, the samples were cooled to 40 °C at a rate of 10 °C/min, and heated once more. For assessing the effects of ageing on the polymer thermal properties, the relevant thermal properties, including glass transition temperature (T_g), melting temperature (T_m) and associated melting enthalpy (ΔH_m) of the polymers, were determined from the first heating cycle to better reflect the material original structure. CF presence could further impact crystallisation behaviour, warranting future investigation. Each measurement was repeated three times. The degree of crystallinity χ_c was calculated according to :

$$\chi_c = \frac{\Delta H_m}{\Delta H_m^\circ} \tag{1}$$

with ΔH_m°, the theoretical melting enthalpy of a fully crystalline sample reported to be 80 J/g for PPS [23] and 130 J/g [18,31] for PEEK.

2.3.4. Chemical characterisation

The Energy Dispersive X-ray (EDX) mode of the SEM (Hitachi TM3000, Hitachi High-Technologies, Japan) was used to obtain the elemental composition on the same sample regions used for SEM but at a lower magnification of 2000× to cover a wider field of view. Before EDX analysis, the samples were dried in an oven set at 120 °C overnight. Elemental composition was measured at 12 distinct points per sample, differentiating between polymer-rich regions (represented in green or blue in the images) and carbon fibre-rich regions (in bright red). This targeted approach was chosen to precisely distinguish between the two phases rather than relying solely on elemental mapping. The average atomic C/O ratio for the polymer-rich regions was calculated and plotted with its standard deviation. The depth resolution of EDX is 1 μm. Attenuated Total Reflectance — Fourier Transform Infrared spectroscopy (ATR-FTIR) measurements were produced with a model Spectrum One (Perkin-Elmer, Germany) using ATR (attenuated total reflectance). Here, the analysis is performed on pure polymer film specimens which underwent an initial drying process within an oven set at 120 °C overnight. This preliminary treatment was implemented to mitigate the influence of water absorption compared to polymer chain degradation during the ageing procedure. Measurements were obtained using the absorbance mode, in the spectral region of 450 to 4000 cm^{-1} at a resolution of 4 cm^{-1} and 100 accumulations. The data

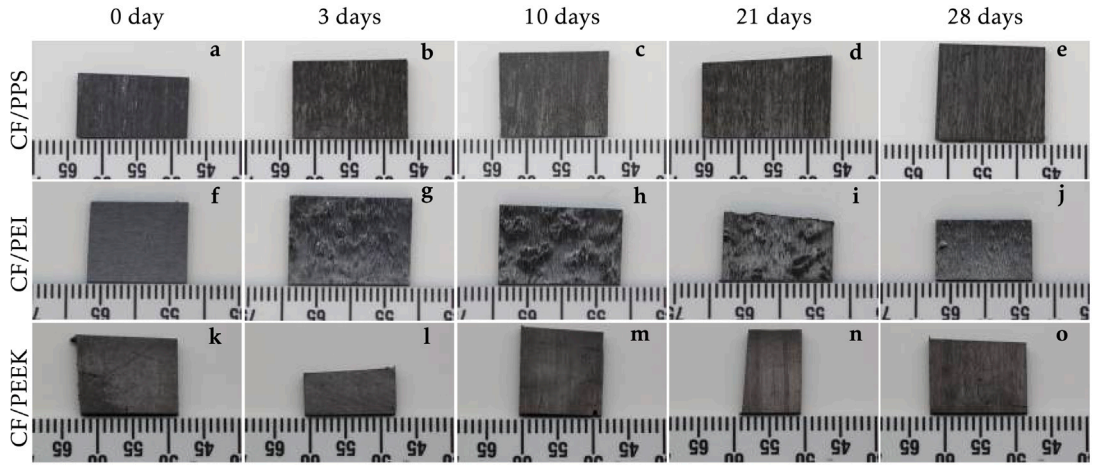

Fig. 1. Photograph of (a)–(e) CF/PPS, (f)–(j) CF/PEI, and (k)–(o) CF/PEEK at initial state and different combined UV radiation/condensation exposures.

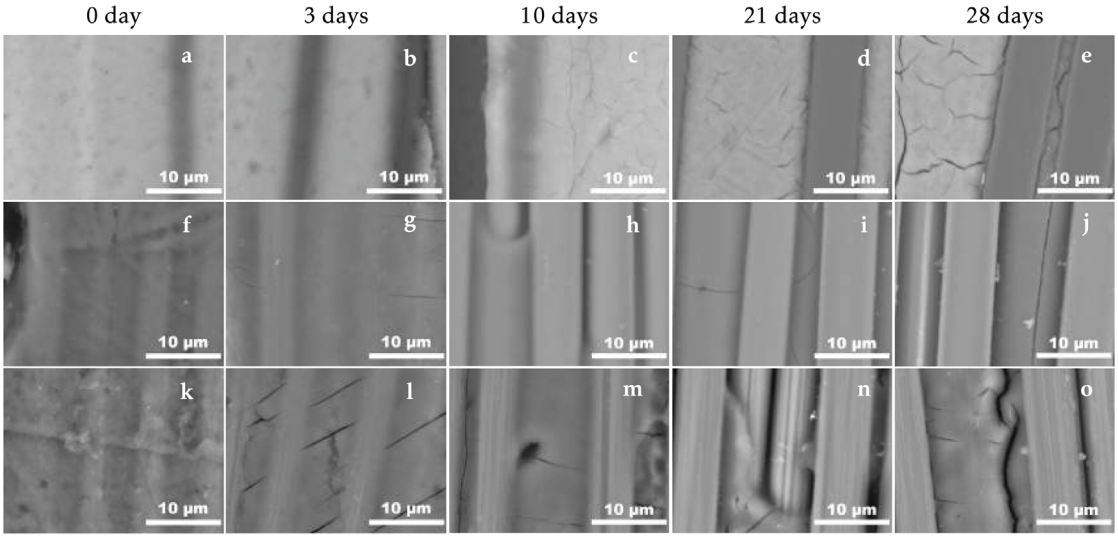

Fig. 2. SEM micrographs of (a)–(e) CF/PPS, (f)–(j) CF/PEI, and (k)–(o) CF/PEEK surfaces before and at different UV radiation/condensation exposures using a BSE detector.

were baseline-corrected and normalised. Specifically, the PPS samples were normalised relative to the peak intensity observed at 1470 cm^{-1}, whereas normalisation for the PEI samples was anchored to the peak at 1495 cm^{-1}, and at 1595 cm^{-1} for PEEK.

3. Results and discussion

3.1. Surface morphology analysis

In the early stages of ageing, photooxidation is visually manifested by discolouration of the sample, which is caused by oxidation of the molecular chains after exposure to UV radiation [32]. As shown in Fig. 1(a–e) and (k–o), surface discolouration was observed on the CF/PPS and CF/PEEK specimens. It can be seen that after 3 and 10 days, the composite surfaces take on a shade of brown. After 21 days, the CF/PPS and CF/PEEK samples became shinier and rougher, suggesting that the polymer matrix was being removed, leaving the carbon fibres bare. In the CF/PEI case (Fig. 1(f–j)), the polymer does not change colour with increasing exposure, but the surface became rougher and shinier after only 3 days of exposition, which also suggests an early erosion of the polymer matrix.

However, upon closer examination using a SEM in Fig. 2, the degradation mechanisms of CF/PPS, CF/PEI, and CF/PEEK begin to diverge. Initially, the surfaces of all unaged thermoplastic composite specimens were covered uniformly by a polymer matrix and no carbon fibres were exposed. Yet, as UV radiation and condensation exposure increases, cracks and cavities start to form and carbon fibres are revealed at the surface.

In the case of CF/PPS, the degradation mechanism can be visualised in Fig. 2(a–e). At 3 days of exposure (Fig. 2b), carbon fibres become more prominent on the surface, while the polymer matrix exhibits no noticeable defects. After 10 days, fine cracks start to form and propagate within the polymer matrix and along the carbon fibre. This is indicative of polymer matrix degradation, where the polymer is gradually eroded away from the carbon fibres (Fig. 2(d–e)). This phenomenon arises from the excessive brittleness of the polymeric matrix. With prolonged exposure, the cracks are more important and severe debonding is observed between the matrix and the fibres. Comparable behaviours were described for epoxy and PPS composites [12,24]. Unlike for CF/PPS, damages in the form of linear thin cracks appear after only 3 days on the polymer matrix of CF/PEI composites (Fig. 2g). As exposure increases (Fig. 2(g–j)), the polymer matrix continues to erode rapidly around the carbon fibres, although the concentration of cracks remains low and does not appear to be localised around the carbon fibres. Additionally, small cavities begin to form at the crack sites (see Fig. 2i). CF/PEEK specimens exhibit the most significant surface damage to the polymer matrix (Fig. 2(k–o)). Large, deep cracks develop after just 3 days of UV exposure and seem to propagate between carbon

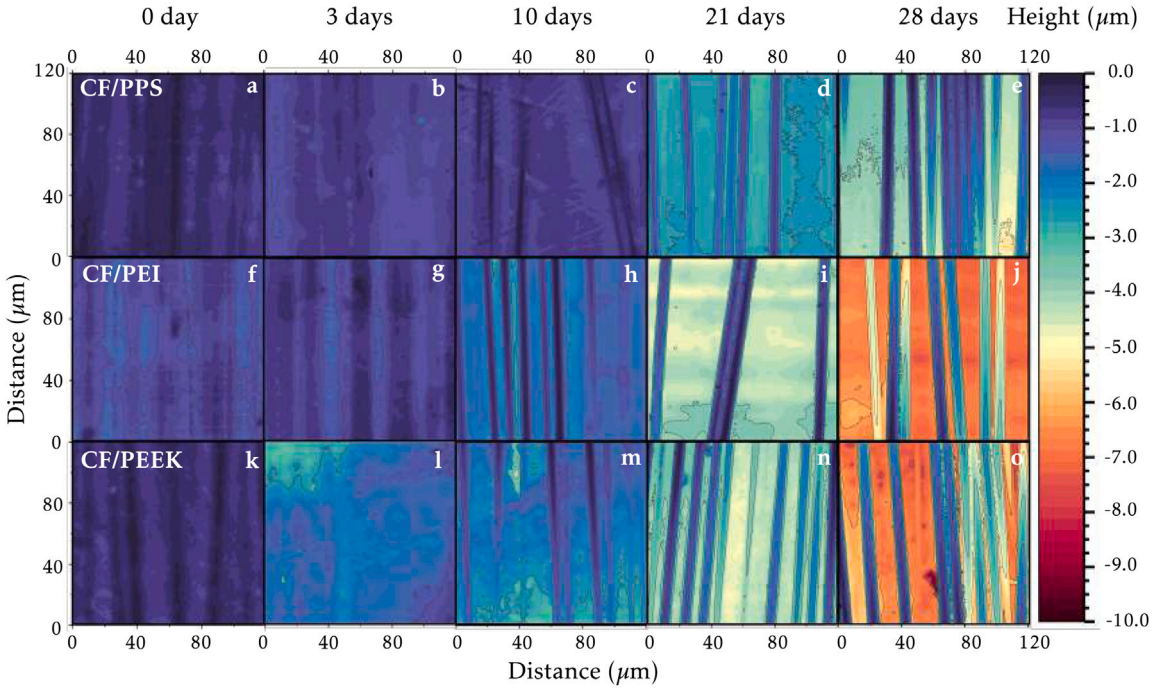

Fig. 3. 2D roughness map of (a)–(e) CF/PPS, (f)–(j) CF/PEI, and (k)–(o) CF/PEEK before and after different UV radiation/condensation exposures using confocal microscopy.

fibres. With extended UV exposure, cavities form within the polymer matrix, and delamination at the interface between the carbon fibres and the matrix becomes more pronounced, leading to further matrix erosion.

It is noteworthy that two distinct crack patterns are observed. On the one hand, CF/PEEK and CF/PEI both develop parallel cracks that remain isolated from one another. This type of crack is characteristic of brittle fracture of the material. In contrast, CF/PPS exhibits "channelled" cracks, where the cracks appear to propagate and branch, forming an interconnected network and are usually observed in a more ductile material. Crack formation is initiated by internal stresses that develop within the materials. Under UV radiation, surface damage occurs, altering the chemical structure of the materials. This degradation can lead to a reduction in chain mobility due to cross-linking or oxidative degradation, hence increasing the stiffness of the material. During condensation, damage is caused by water diffusion in the material. If the material is hygroscopic, it will be prone to water absorption leading to deformation through swelling. As different regions of the material degrade non-uniformly under UV exposure, uneven swelling occurs, leading to differential expansion within the material that generates internal stresses. Examining water absorption at saturation of the different polymer matrix, PEI exhibits the highest hygroscopicity with 2.9% of water uptake, followed by PEEK at 1.65%, and PPS at just 0.6%. This behaviour is consistent with their molecular structures, as PEI and PEEK contain ketone and ether groups that interact strongly with water molecules. Therefore, during weathering exposure, the damage caused to CF/PEI and CF/PEEK by UV radiation is exacerbated by condensation as it favours water diffusion into the structure, hence increasing internal stresses and promoting brittle fractures [33]. Moreover, thermal residual stresses from processing can exacerbate the cracking behaviour of the different composites. CF/PPS has the lowest processing temperature at 315 °C, followed by CF/PEI and CF/PEEK at 380 °C. All samples were rapidly cooled during compression in the press. The significant temperature processing differences between CF/PEI, CF/PEEK, and CF/PPS can induce thermal residual stresses, which may affect the polymer's crystallinity and mechanical properties, such as brittleness [30,34], further playing a role in crack formation and propagation.

The polymer matrix of all thermoplastic composites is affected by UV radiation and condensation, leading to surface erosion and a weakening of the bond between fibres and matrix. As the mechanical properties of a composite depend on the integrity of the reinforcement-matrix bond, the debonding initiated by UV radiation may cause premature failure of certain fibres under applied stress. Consequently, it is crucial to quantify the depth of polymer matrix degradation. Here, confocal microscopy is used to determine the depth of removal of the polymer matrix by generating 2D roughness maps (Fig. 3), surface profiles (Fig. 4), average maximum penetration depths (Fig. 5), and surface roughness (Ra) (Fig. A.1). The 2D roughness maps in Fig. 3 represent the surface topography of each thermoplastic composite at different UV radiation/condensation exposure times, showing the changes in surface height across the samples. The results indicate that the matrices of CF/PEI (Fig. 3(f–j) and Fig. 4b) and CF/PEEK (Fig. 3(k–o) and Fig. 4c) were removed more rapidly than that of CF/PPS (Fig. 3(a–e) and Fig. 4a). After just 3 days of UV exposure, matrix removal reaches 2.3 μm, increasing to 7.8 μm for CF/PEEK and 6.8 μm for CF/PEI after 28 days (Fig. 5). Carbon fibres become significantly visible after 10 days (Fig. 3 h and m). As exposure time progresses, the polymer matrix erosion is observed to be uneven, with the formation of valleys and deep cavities. In contrast, CF/PPS undergoes a two-step process with negligible removal of PPS matrix (1.4 μm) up to 10 days of UV exposure, followed by a steeper increase to 4.7 μm after 28 days (Figs. 4a and 5).

3.2. Chemical degradation

To fully understand the effect of long-term exposure to environmental weathering on composite materials, it is necessary to recognise that damage extends beyond structural deterioration. These materials also experience significant chemical changes, affecting their performance and durability. EDX analysis of CF/PPS composites highlights how the elemental composition evolves under varying UV radiation and condensation exposures (see Figs. 6(a)(I–III) and 6(b)). Two distinctive regions are observed, with a polymer-rich region in green due to the presence of sulphur and carbon fibre-rich region in red. The polymer-rich region in the reference CF/PPS comprises 85.5% ± 0.5 carbon

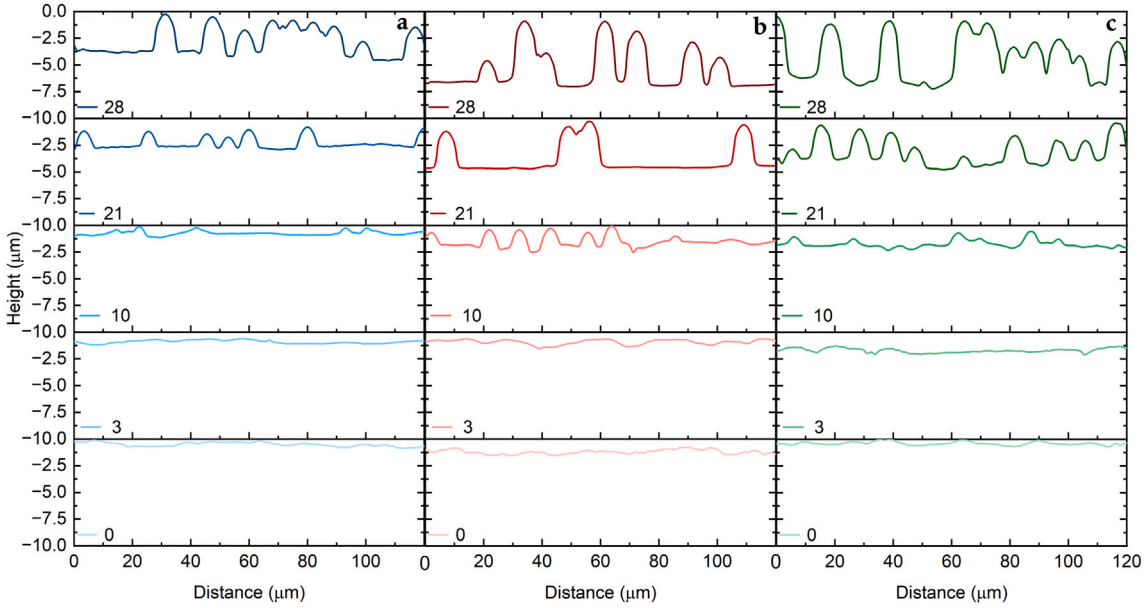

Fig. 4. Roughness profile of (a) CF/PPS, (b) CF/PEI, and (c) CF/PEEK surfaces at initial state and after different UV radiation/condensation exposures (days), using confocal microscopy.

Table 2
Elemental composition analysis (carbon, sulphur, nitrogen and oxygen) of CF/PPS, CF/PEI and CF/PEEK laminates before and after weathering exposure.

Exposure	Elemental atomic %							
days	CF/PPS			CF/PEI			CF/PEEK	
	Polymer rich region							
	C%	O%	S%	C%	O%	N%	C%	O%
0	85.5 ± 0.5	0.0	14.5 ± 0.5	81.9 ± 1.0	12.8 ± 0.7	5.3 ± 0.4	88.0 ± 0.6	12.0 ± 0.6
3	79.7 ± 0.7	7.1 ± 0.6	13.1 ± 1.0	79.6 ± 1.1	14.9 ± 1.1	5.6 ± 0.7	85.5 ± 0.9	14.5 ± 0.9
10	79.1 ± 1.6	7.4 ± 1.4	13.5 ± 0.7	79.5 ± 5.8	14.2 ± 5.0	6.3 ± 1.1	84.8 ± 1.8	15.2 ± 1.8
21	78.0 ± 1.2	8.9 ± 0.7	13.1 ± 0.5	78.8 ± 1.9	17.0 ± 1.1	4.1 ± 2.8	83.3 ± 1.3	16.7 ± 1.3
28	79.2 ± 0.8	8.3 ± 1.3	12.5 ± 1.7	80.5 ± 7.3	12.3 ± 8.3	7.2 ± 1.0	84.1 ± 2.0	15.9 ± 2.0
	Carbon fibre rich region							
0	98.0 ± 0.5	0.0	2.0 ± 0.5	85.6 ± 2.0	10.6 ± 1.5	3.9 ± 3.3	92.4 ± 0.8	7.6 ± 0.8
3	94.7 ± 3.0	3.5 ± 1.9	1.8 ± 1.1	87.2 ± 2.4	5.4 ± 2.3	7.5 ± 0.2	92.1 ± 1.1	7.9 ± 1.1
10	94.9 ± 3.9	4.3 ± 3.0	0.8 ± 0.8	89.2 ± 1.0	2.8 ± 0.5	8.1 ± 0.6	95.5 ± 2.5	4.5 ± 2.5
21	97.7 ± 0.9	2.1 ± 0.8	0.2 ± 0.1	90.2 ± 2.2	3.8 ± 3.3	6.0 ± 2.2	97.9 ± 1.9	2.1 ± 1.9
28	98.4 ± 0.6	1.6 ± 0.6	0.1 ± 0.1	90.0 ± 1.9	2.7 ± 1.1	7.4 ± 1.1	97.8 ± 1.3	2.2 ± 1.3

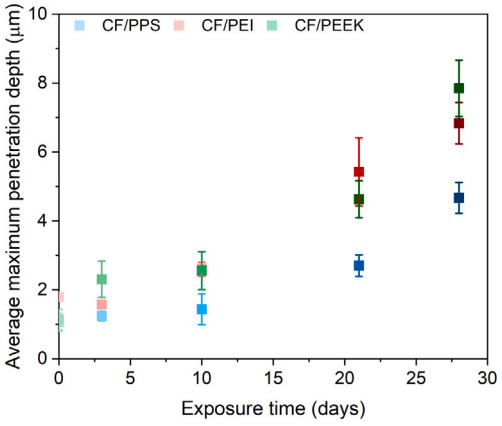

Fig. 5. Average maximum penetration depth on CF/PPS, CF/PEI, and CF/PEEK surfaces at initial state and after different UV radiation/condensation exposures (days), using confocal microscopy.

and 14.5% ± 0.5 sulphur, with no detectable presence of oxygen (Table 2). In the carbon fibre-rich region (red), 98% ± 0.5 of carbon and 2% ± 0.5 sulphur is detected, indicating the presence of a thin layer of polymer covering the carbon fibre. To quantify the oxidative degradation of the composites, the oxygen-to-carbon ratio (O/C) was calculated (Fig. 6(b)). The O/C ratio increases rapidly, reaching 8.9% in the polymer-rich zone after just three days of exposure and peaking at 11.4% after 21 days. This indicates that once the polymer undergoes a certain degree of degradation, it detaches from the matrix and carbon fibre surface. In the carbon fibre-rich region, the amount of oxygen reached 4% after 10 days of exposure (Table 2), but after 28 days, the sulphur had disappeared, and oxygen levels dropped to 1.5%, indicating extensive polymer degradation and its entire removal from the fibre surface.

For CF/PEI, EDX analysis (Fig. 6(a)(IV–VI) and Table 2) showed an initial composition of 81.9% ± 1.0 carbon, 12.8% ± 0.7 oxygen, and 5.3% ± 0.7 nitrogen in the polymer-rich region (blue), and 85.6% ± 2.0 carbon, 10.6% ± 1.5 oxygen, and 3.9% ± 3.3 nitrogen in the carbon fibre-rich region (red). Similarly to CF/PPS, the undamaged CF/PEI has a uniform thin layer of polymer on the surface. However, the oxygen content in the polymer-rich zone increased to 14.9% ± 1.1 after three days of exposure (see Fig. 6(b) and Table 2). Gradually, the

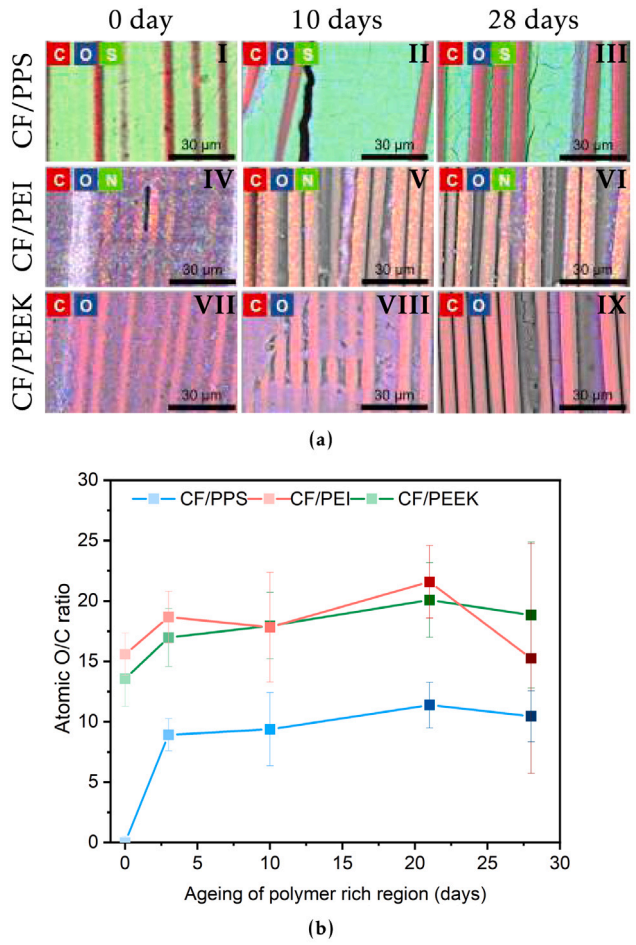

Fig. 6. (a) Chemical mapping of (I–III) CF/PPS, (IV–VI) CF/PEI and (VII–IX) CF/PEEK surfaces in their initial state and after different UV radiation/condensation exposures, using EDX analysis. Elements quantified for CF/PPS are carbon (red), sulphur (green) and oxygen (blue), for CF/PEI, carbon (red), nitrogen (green) and oxygen (blue), while for CF/PEEK, carbon (red) and oxygen (blue). (b) The effect of UV radiation/condensation exposures on oxygen to carbon ratio in the polymer matrix-rich region.

oxygen content rise to 17% ± 1.1 after 21 days, which is indicative of oxidative degradation occurring (see Fig. 6(b)). A subsequent decrease in oxygen content at 28 days is attributed to the lack of signal due to the strong erosion of the PEI matrix. In the carbon fibre-rich region, oxygen content decreased from 10.6% to 2.7%, indicating substantial polymer removal from the fibre surface, which is in agreement with the results obtained in Figs. 4b and 5. The elemental composition of CF/PEEK is 88% ± 0.6 carbon, and 12% ± 0.6 oxygen for the polymer rich-region (blue), and 92.4% ± 0.8 carbon, and 7.6% ± 0.8 oxygen for the carbon fibre rich-region (red) (Fig. 6(a)(VII–IX) and Table 2). Similarly to CF/PPS and CF/PEI, a uniform polymeric layer is observed at the surface before starting the weathering process. The polymer-rich region exhibited a steady increase in oxygen content, with an initial O/C ratio of 13.6%, and reached 20.1% after 21 days of exposure (see Fig. 6(b)). Meanwhile, the carbon fibre became bare with a drop to 2.2% of oxygen content on its surface. Similarly to CF/PEI, the decrease in oxygen content at 28 days on the polymer matrix is due to erosion and a weak signal.

FTIR provides additional insights into the chemical degradation of the pure polymer during the ageing process. The band allocation of the different polymers is described in Table 3. All samples were previously dried to mitigate the influence of water absorption compared to polymer chain degradation on the measurement. The use of pure polymer films was necessary to accurately identify degradation

Table 3
Allocation of FTIR bands for PPS, PEI and PEEK.

Polymers	Wavelength (cm^{-1})	Peak allocation
PPS [35]	1384–1574	C=C characteristics of phenyl ring vibrations
	1180	C–H deformation in the bending plane
	1074–1092	C–S bending
	805	C–H out-of-plane bending deformation
PEI [36]	1714–1773	C=O symmetrical and asymmetrical stretching
	1408–1591	C=C phenyl ring vibrations
	1356	C–N stretching
	1240	C–O–C stretching
	1070, 743	C–N ring deformation
PEEK [37]	1653	C=O stretching
	1593, 1500, 1485 & 1410	C=C phenyl ring vibrations
	1305	(C–C(=O)–C) bending
	1217 & 1184	C–O–C stretching
	600–1200	C–H deformation

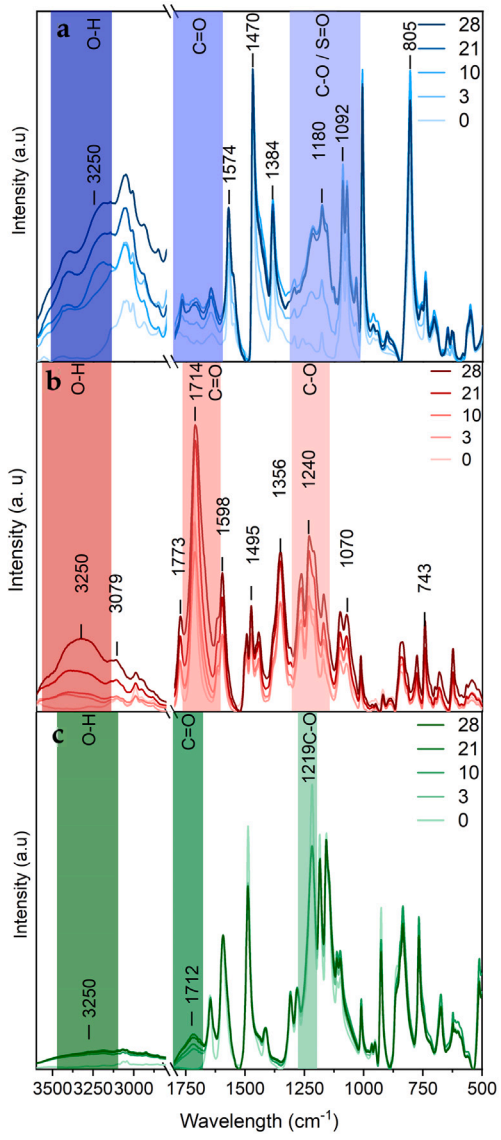

Fig. 7. ATR FTIR spectra of (a) PPS, (b) PEI and (c) PEEK surfaces in their initial state and after different UV radiation/condensation exposures (days).

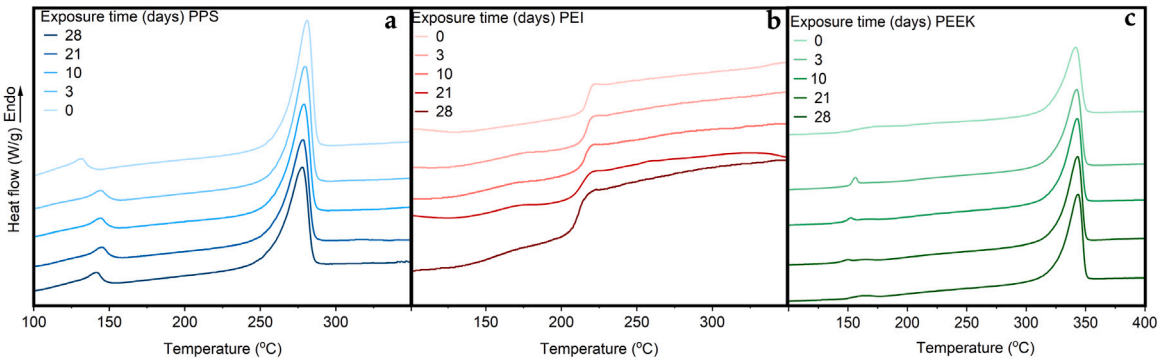

Fig. 8. Thermograms of the first heating cycle for (a) PPS, (b) PEI, and (c) PEEK at initial state and after different UV radiation/condensation exposures (days).

mechanisms, such as chain scission and oxidation, without interference from carbon fibres, which could otherwise attenuate signal intensity. For PPS, the reference spectrum in Fig. 7a shows characteristics C–C stretching vibrations of the phenyl ring at 1384, 1470 and 1574 cm^{-1}. Peaks corresponding to in-plane C–S stretching vibrations and C–H vibrations of the benzene backbone are detected at 1074, 1092 cm^{-1} and 830 cm^{-1}, respectively [35]. With increasing weathering, new intense absorption peaks in the phenolic group region (3200–3400 cm^{-1}) and carbonyl region (1650–1800 cm^{-1}) appear (Fig. 7A). The broadening of the carbonyl peaks indicates the formation of several carbonyl species, such as aldehydes, carboxylic acids and esters. In addition, the increase in intensity of the peaks between 1150 and 1300 cm^{-1}, representative of ether and sulphonic group, increases compared to the phenyl peak at 1470 cm^{-1}, suggesting progressive chemical alteration of the polymer chain [38,39].

For PEI, the FTIR spectra also revealed significant changes after environmental exposure (Fig. 7b and Table 3). The initial spectrum of PEI displayed characteristic peaks associated with the imide group, including the C=O stretching vibration at 1714–1773 cm^{-1}, C=C bond of the phenyl ring at 1356–1598 cm^{-1}, C–N stretching at 1356 cm^{-1}, and C–O–C stretching at 1240 cm^{-1}. In addition, the C–N deformation of the imide ring is identified at 1070 and 743 cm^{-1} [36]. After UV radiation and condensation ageing, the PEI polymer matrix shows significant changes in its molecular structure. The increase and broadening of peaks in the hydroxyl region (3200–3400 cm^{-1}), the carbonyl region (1650 cm^{-1}) and the ether region (1150–1300 cm^{-1}) indicate oxidative degradation, of the polymer backbone. In PEEK, the reference spectrum in Fig. 7c exhibits the characteristic C–C stretching vibrations of the phenyl rings at 3070, 1470 and 1574 cm^{-1}, C=O stretch vibrations of the aromatic ketones at 1645 cm^{-1}, and the C–O vibration of the ether. As for PEI, the increase in UV radiation and condensation, the FTIR spectra showed a steady broadening and increase in absorption associated with carbonyl groups (1712 cm^{-1}) and hydroxyl groups (3200–3400 cm^{-1}), indicative of oxidation and hydrolysis reactions, respectively [19]. However, at 1217 and 1184 cm^{-1}, the asymmetric stretching of the diphenyl ether group decreases in intensity, which could be linked to chain scission [40]. To summarise, FTIR analysis corroborates the EDX findings by highlighting oxidative and hydrolytic degradation processes in these polymer matrices.

3.3. Impact of ageing on thermal and mechanical properties

After assessing the influence of weathering conditions on the morphology and chemical structure of the composites, it is crucial to explore how this affects their thermal and mechanical properties. The alterations to the polymer matrix induced by prolonged exposure to UV radiation and moisture often influence the composite's overall performance, resulting in potential reductions in thermal stability, fatigue resistance, mechanical strength, and long-term viability.

Table 4
T_g, T_m, temperature of crystallisation (T_c) and degree of crystallinity (χ_c) of PPS, PEI and PEEK before and after UV radiation/condensation exposure during first thermal heating and cooling.

Polymers	Exposure time days	T_g °C	T_m °C	T_c °C	χ_c %
PPS	0	128.7 ± 1.7	281.1 ± 0.1	231.8 ± 2.2	54.6 ± 1.3
	3	140.9 ± 1.1	279.8 ± 0.2	239.5 ± 1.0	53.3 ± 0.7
	10	141.4 ± 0.4	278.9 ± 0.1	242.4 ± 0.3	52.2 ± 0.23
	21	142.1 ± 0.5	279.8 ± 2.1	244.6 ± 0.5	51.3 ± 1.4
	28	138.2 ± 1.3	277.5 ± 0.2	240.7 ± 0.8	50.4 ± 1.2
PEI	0	216.7 ± 0.3			
	3	215.6 ± 0.4			
	10	215.3 ± 0.6			
	21	211.7 ± 2.0			
	28	211.5 ± 0.8			
PEEK	0	156.3 ± 0.1	341.7 ± 0.2	298.2 ± 0.5	35.2 ± 1.8
	3	150.08 ± 0.4	342.5 ± 0.4	298.8 ± 0.6	39.6 ± 1.0
	10	147.04 ± 1.1	343.0 ± 0.7	303.2 ± 0.4	41.4 ± 1.2
	21	144.5 ± 0.6	343.3 ± 0.2	304.3 ± 0.4	40.6 ± 0.8
	28	153.3 ± 1.2	343.7 ± 0.6	303.1 ± 0.2	41.0 ± 1.1

The degree of crystallinity in this study was determined using pure polymer films. It is well-established that the presence of carbon fibres influences the crystallinity of the polymer matrix. For instance, Lee and Porter [41] demonstrated that in PEEK composites, CF acts as a nucleating agent, increasing the crystallinity by approximately 3%. Similarly, Oshima et al. [34] investigated the effect of temperature on the crystallisation behaviour of PPS and CF/PPS composites. Their study revealed that the addition of CF enhances the crystallinity of the polymer, which is attributed to the heterogeneous nucleation of crystals, specifically through epitaxial growth from the fibre surface. Although the absence of CF alters the proportion of crystalline and amorphous phases in the polymer matrix, the degradation mechanisms occurring within each phase, such as chain scission and oxidation, remain fundamentally the same. Therefore, even if the phase ratio differs, the observed trends in the evolution of each phase still provide valuable insight into the underlying degradation behaviour of the material. This allows for meaningful interpretation of ageing phenomena, even in the absence of reinforcement. Figs. 8a and B.3 present the heating thermograms showing the evolution of the melting (T_m) and glass transition (T_g) temperatures of PPS samples before and after ageing, while Fig. B.2(a) shows the corresponding cooling thermograms. The ageing behaviour of PPS reveals a complex degradation mechanisms that significantly affect its thermal and structural properties. T_g increased by 13.4 °C after just 3 days of exposure, reaching a maximum of 142.1 ± 0.5 °C at 21 days, before slightly declining to 138.2 ± 1.3 °C at 28 days. The initial rise in T_g is attributed to increased chain packing and reduced molecular mobility. The subsequent decrease suggests chain scission, which reduces rigidity [42].

The progressive decrease in crystallinity, from 54.6% ± 1.3 at day 0 to 50.4% ± 1.2 at day 28, reflects the gradual disruption of

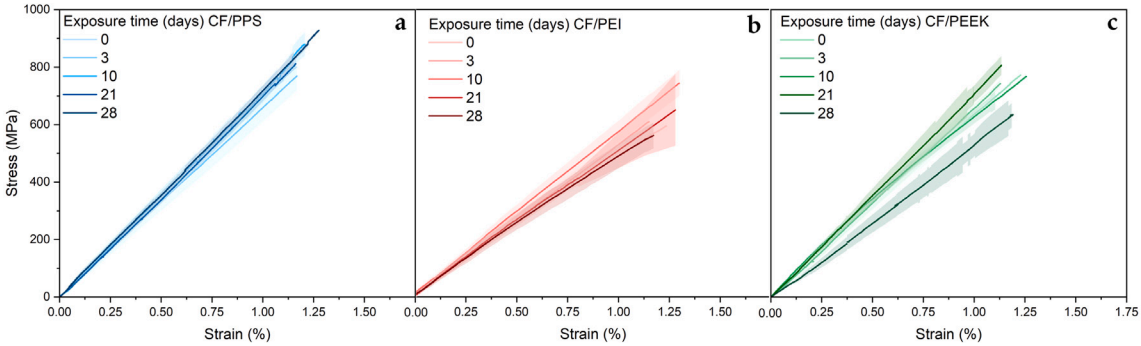

Fig. 9. Average stress–strain curve for (a) CF/PPS, (b) CF/PEI, and (c) CF/PEEK at different UV radiation/condensation exposures (days).

crystalline domains, likely caused by oxidative degradation, causing branching and/or cross-linking. These processes, accelerated by moisture and oxygen through radical formation, hinder the polymer's ability to crystallise [43]. The concurrent drop in T_m, from 281.1 ± 0.1 °C to 277.5 ± 0.2 °C, reinforces this loss of structural order. Together, the reductions in T_m and crystallinity indicate a shift towards a more amorphous state, driven by the interplay of chain scission and oxidative cross-linking that impairs reorganisation into ordered domains.

Overall, the thermal response of aged PPS results from the competing effects of physical ageing, chain scission, cross-linking, and the formation of oxidative degradation products such as ketones, aldehydes, and esters [44]. These variations in crystallinity, in parallel with the onset of cross-linking/branching, are likely to have a significant influence on the mechanical behaviour of the material.

For PEI in Fig. 8b, the glass transition temperature (T_g) of PEI decreases significantly with increasing exposure time, from 216.7 ± 0.3 °C to 211.5 ± 0.8 °C (see Table 4). This suggests that chain scission is the main degradation mechanism, as the formation of end-group regions increases free volume and chain mobility, reducing T_g [45].

Figs. 8c and B.2(b) show the first heating and cooling thermograms for PEEK. Initially, T_g decreases from 156.3 ± 0.1 °C to a minimum of 144.5 ± 0.6 °C after 21 days of exposure, suggesting increased chain mobility due to chain scission. This process reduces the molecular weight, enhancing segmental mobility and facilitating reorganisation into more ordered structures. Consequently, χ_c rises rapidly from 35.2% ± 1.8 to 39.6% ± 1.0 within the first 3 days, stabilising at 41.4% ± 1.2 by day 10 (see Table 4). The increase in crystallinity is further corroborated by the rise in T_c from 298.2 ± 0.2 °C to 303.2 ± 0.4 °C (see Fig. B.2(b) and Table 4), indicating that shorter chains crystallise at higher temperatures due to enhanced mobility and nucleation efficiency.

However, T_g increases to 153.3 ± 1.2 °C by day 28, implying that chain mobility is restricted. Simultaneously, T_m exhibits a gradual increase, reaching 343.7 ± 0.6 °C at 28 days, reflecting on the formation of a stable crystalline domains. Previously, Mylläri et al. [19] reported that UV irradiation only had no discernible effect on χ_c or T_m of the tested PEEK fibres. However, degradation was localised in the amorphous regions of the polymer, as evidenced by the drop then increase in T_g with exposure time, suggesting an initial loss of mobility followed by structural reorganisation. Here, UV radiation is combined with condensation, changing the degradation mechanism affecting both the amorphous and crystalline phases. Moisture promotes chain scission and termination up to 21 days of exposure, improving chain mobility and crystallisation [21,22].

In summary, while both PPS and PEEK undergo chain scission and oxidation during UV and moisture ageing, PEEK becomes more crystalline and thermally stable due to reorganisation of shorter chains, whereas PPS loses crystallinity and thermal stability, transitioning towards a more amorphous structure.

The mechanical properties of composite materials are strongly influenced by the compatibility between the polymer matrix and the reinforcing fibre. Previous analyses of CF/PPS, CF/PEI and CF/PEEK composites have shown that UV radiation and condensation ageing lead to chemical degradation, fibre delamination and microstructural changes. However, these degradations remained superficial, with, for example, a maximum of 7.8 μm of polymer matrix removal after 28 days of exposure (Fig. 5). Therefore, it is crucial to understand if these factors affect the mechanical properties of the composite material as a whole when used under standard engineering applications. The cross-ply specimens selected for this study have the same configuration as those used in the design process and are employed here to validate that the material remains suitable for mechanical applications despite ageing. It is worth mentioning that other methods such as transverse tension, shear, fracture toughness, or configuration (45°), would provide more direct insights into matrix degradation.

The stress–strain curves for both unaged and aged CF/PPS samples with a $[0,90]_{3s}$ configuration are shown in Fig. 9a, where the composite exhibits consistently brittle fracture behaviour. A closer examination of the elastic modulus E in Fig. 10(a) reveals a small decrease from 71.4 ± 3.1 to 64.6 ± 0.7 GPa. The tensile strength as shown in Fig. 10(b) rises from 790 ± 34 MPa to 864 ± 41 MPa, which at first may seem counterintuitive given the concurrent increase in brittleness. However, this behaviour could be partly explained with molecular-level changes caused by UV exposure.

The tensile fracture morphology of CF/PPS, observed in Fig. 11(a), shows that the unaged sample undergoes brittle fracture, specifically of the LGM-type as described in ASTM D3039/D3039M-17. This fracture is characterised by lateral cracks at the gauge section and in the middle of the sample. With increasing exposure, the fracture morphology evolved, showing a high density of cracks on the surface and delamination around the fracture site. This indicates that the degradation process leads to localised embrittlement, most likely due to increased cross-linking and partial chain scission. The cross-linking stiffens the matrix and enhances strength, while the chain scission reduces the overall toughness, explaining the observed combination of increased strength and brittleness. Furthermore, the changes in crystallinity also play a role in the mechanical behaviour. As indicated by the DSC results in Fig. 8a, the increase in glass transition temperature (from 128.7 °C to 140.9 °C) after 3 days of UV exposure suggests the onset of cross-linking reactions or the removal of residual low-molecular-weight species. This structural reorganisation may enhance the stiffness of the matrix, temporarily contributing to improved tensile strength. However, with prolonged exposure (28 days), degradation mechanisms such as delamination and fibre–matrix debonding become dominant, leading to a decrease in mechanical performance.

Fig. 9b shows the longitudinal tensile stress and strain curves for CF/PEI ($[0,90]_{4s}$) at different ageing times. In all states, the behaviour of the composite exhibits brittle fracture characteristics. The unaged CF/PEI measurements demonstrate repeatability and minimal variation in tensile strength at failure. As shown in Fig. 11(b), the unaged CF/PEI sample undergoes a brittle fracture and has a tensile strength of 574 ± 63 MPa (see Fig. 10(b)) and an elastic modulus (E) of

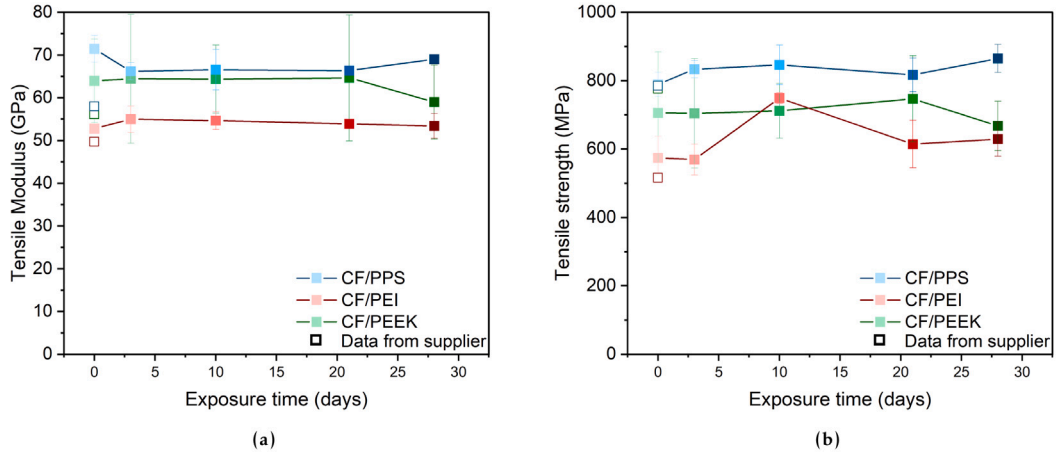

Fig. 10. Average values for (a) modulus of elasticity (E) and (b) fracture toughness for CF/PPS, CF/PEI, and CF/PEEK at initial state and different UV radiation/condensation exposures (days).

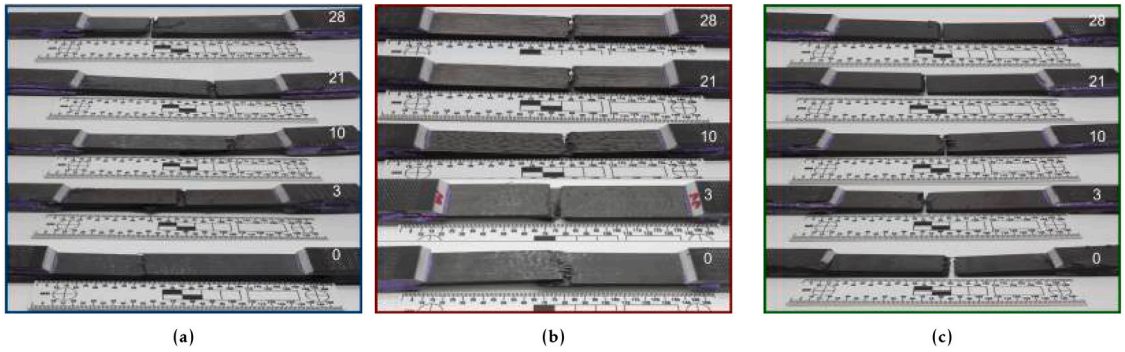

Fig. 11. Photographs of the fracture morphology of (a) CF/PPS, (b) CF/PEI and (c) CF/PEEK in their initial state and after different UV radiation/condensation exposures (days).

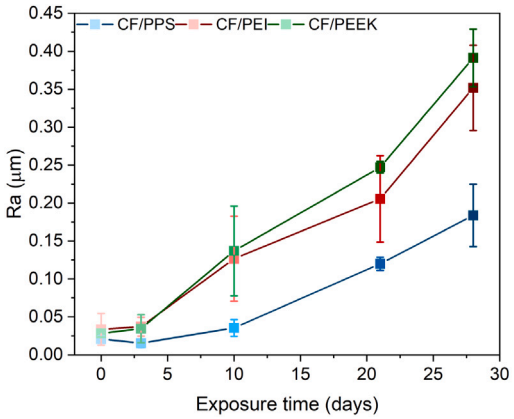

Fig. A.1. Evolution of Ra CF/PPS, CF/PEI, and CF/PEEK surfaces at initial state and after different UV radiation/condensation exposures (days), using confocal microscopy.

52.75 ± 0.9 GPa (see Fig. 10(a)), which is in line with the data provided by the manufacturer. With increasing exposure, small differences in the mechanical properties can be noticed. A light increase of the modulus, reaching a maximum of 55 ± 3.1 GPa after 3 days, while the tensile strength peaks at 749 ± 16.1 MPa after 10 days. It is important to note that although the tensile strength at break and elastic modulus after 10 days show higher values than the unaged specimen, the results are more scattered. This variability suggests unpredictability that must be taken into account for safety reasons. In Fig. 11(b), the type of fracture changes with exposure time. As it increases, the fractures become less fragile and show signs of delamination. This can be attributed to a reduction in the degree of bonding between the fibres and the resin. Although the fibres themselves are less affected by ageing, the overall load-bearing capacity of the composite relies on the strength of the bond between the reinforcement phase and the matrix phase. The disbonding of fibres from the surface layer of the matrix leads to premature failure of some fibres under tension, compromising the mechanical integrity of the composite [46]. This causes variation between samples and increases unpredictability, which could lead to premature failure of the composite. In the case of CF/PEI, the variation in repeatability peaked after 21 days and then began to stabilise.

The tensile strength for the unaged CF/PEEK specimen ($[0,90]_{4s}$) is 705 ± 179 MPa, increases progressively to 746 ± 125 MPa at 21 days (see Figs. 9c and 10(b)), and drops drastically to 667 ± 72 MPa at 28 days. The calculated E of unaged CF/PEEK is 64 ± 9.8 GPa, remaining constant until 21 days of exposure, finally significantly decreasing to 59 ± 8.6 GPa at 28 days. This behaviour is consistent with a degradation mechanism dominated by chain scission, which was previously observed. As chains break, molecular interaction within the polymer matrix as well as with the surface of the carbon fibres are reduced, hence weakening its ability to withstand tensile loads. Unlike CF/PPS and CF/PEI, the fracture behaviour of CF/PEEK shown in Fig. 11(c) remains stable with no significant increases in cracks and delamination during ageing.

Overall, this test indicates that the carbon fibres remain unaffected by UV radiation with condensation. While minor variations are observed between the aged polymer composites, they should be interpreted with caution. After 28 days, the tensile strength of CF/PPS increased by 9.6% compared to the reference, while E decreased by 3.3%. CF/PEI exhibited a similar improvement in tensile strength

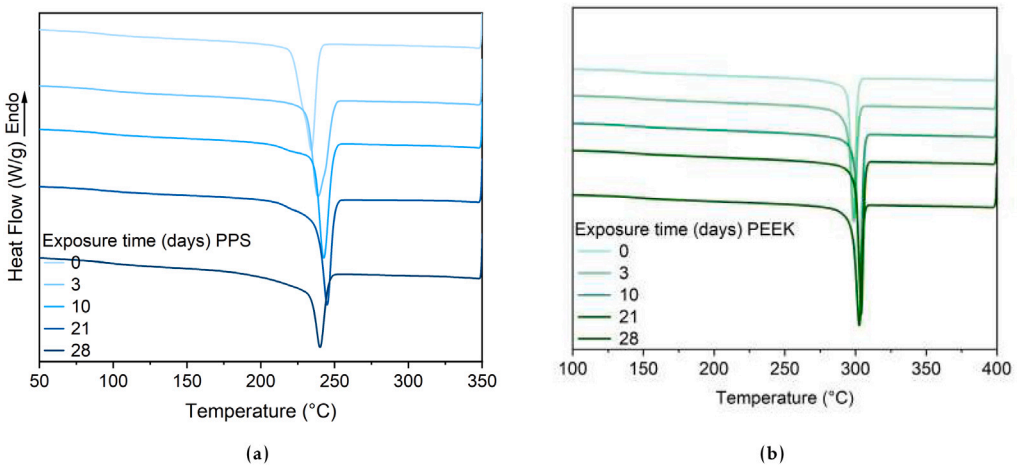

Fig. B.2. Thermograms of cooling cycle for (a) PPS, and (b) PEEK at different UV radiation/condensation exposures.

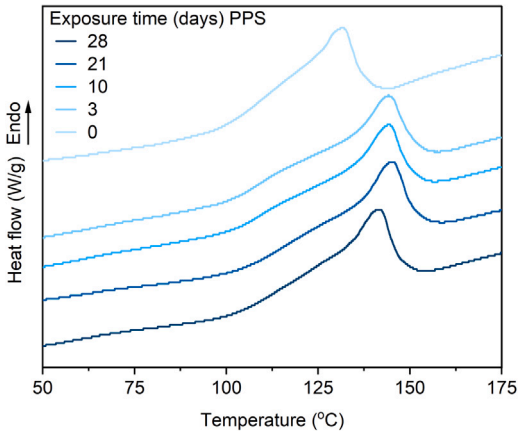

Fig. B.3. Evolution of the T_g for PPS at different exposures.

(9.6%) with a reduction in E (1.2%). In contrast, PEEK experienced a decline in both tensile strength and E with a drop of 5.3% in 7.7%, respectively.

Beyond these changes in properties, maintaining low variance between samples over time is crucial for accurately predicting material behaviour and failure. The repeatability variance of tensile strength was quantified for each composite. CF/PPS exhibited a reference variance of 4%, which increased to a maximum of 7% after 10 days, indicating that despite the property changes over time, the degradation mechanism affects mechanical properties consistently. PEI demonstrated a similar trend, with an initial variance of 11% that peaked at 11.4% after 21 days. In contrast, PEEK showed the highest variability, with a 25% variance between samples.

4. Conclusion

The effects of UV radiation and condensation were evaluated on three distinct carbon fibre-reinforced thermoplastic composites. The study assessed changes in morphology (Figs. 1, 3, 4, 5), fracture behaviour (Fig. 11), and mechanical properties of the composites, as well as the chemical structure (Figs. 6, 7) and thermal properties (Fig. 8) of their corresponding pure polymer matrices. Two principal degradation mechanisms were identified. First, the CF/PPS composite exhibited minimal surface damage following weathering, with only a small amount of polymer matrix removal. Its hydrophobic nature limited water diffusion into the composite, mitigating internal stresses from swelling. The primary degradation mechanism for PPS was cross-linking, as confirmed by both thermal and mechanical property tests. Over prolonged exposure (20–28 days), the degradation rate appeared to stabilise, indicating greater long-term durability. In contrast, CF/PEI and CF/PEEK were more susceptible to UV radiation and condensation, largely due to their hygroscopicity, which induced internal stresses and brittle fractures, resulting in increased exposure of bare carbon fibres and reduced fibre-resin interaction. Their principal degradation mechanism was chain scission. The tensile strength of CF/PPS improved with minimal variance over time, while CF/PEI and CF/PEEK showed higher variability. After 20 days of exposure, both CF/PEI and CF/PEEK underwent substantial chemical degradation, with surface erosion of the polymer matrix reaching approximately 6.8 μm and 7.8 μm, respectively. In contrast, CF/PPS displayed a more stable and gradual degradation mechanism, making it more predictable. This consistent behaviour, combined with its relatively low cost, makes CF/PPS the most reliable and suitable option for applications where long-term environmental durability and performance are critical.

CRediT authorship contribution statement

Annelise Jean-Fulcrand: Writing – original draft, Visualization, Methodology, Investigation, Formal analysis, Data curation. **Ewen Léger:** Formal analysis, Data curation. **Frédéric Dau:** Supervision, Funding acquisition. **Martine Dubé:** Writing – review & editing, Supervision, Resources, Project administration, Funding acquisition, Conceptualization. **Ilyass Tabiai:** Writing – review & editing, Supervision, Resources, Project administration, Funding acquisition, Conceptualization.

Declaration of Generative AI and AI-Assisted Technologies

During the preparation of this work, the authors used ChatGPT in order to improve readability and language. After using this tool, the authors reviewed and edited the content as needed and take full responsibility for the content of the publication.

Declaration of competing interest

The authors declare the following financial interests/personal relationships which may be considered as potential competing interests: Ilyass Tabiai reports financial support was provided by Flying Whales. The other authors have declared that they have no known competing financial interests or personal relationships that could have appeared to influence the work reported in this paper.

Acknowledgements

The authors are thankful to Serge Plamondon for providing assistance during the mechanical tests and Nabil Mazeghrane for his help during the samples preparation. This study was commissioned and supported by FLYING WHALES & LES DIRIGEABLES FLYING WHALES QUEBEC Inc., France and Canada, and was conducted in close collaboration with the company. The authors are also thankful to MEIE, Canada for financial support.

Appendix A. Surface properties: Surface roughness of CF/PPS, CF/PEI, and CF/PEEK

The surface roughness (Ra) was measured by averaging the values obtained from eight lines drawn on each of the two images captured for each sample type and condition.

Appendix B. Thermal properties: Cooling thermograms of PPS and PEEK

Cooling thermograms of PEEK and PEI reveal their crystallisation behaviour and thermal transitions.

Fig. B.3 displays the T_g for PPS.

Data availability

Data will be made available on request.

References

[1] Chen Yonglin, Zhang Junming, Li Zefu, Zhang Huliang, Chen Jiping, Yang Weidong, Yu Tao, Liu Weiping, Li Yan. Intelligent methods for optimization design of lightweight fiber-reinforced composite structures: A review and the-state-of-the-art. Front Mater 2023;10. http://dx.doi.org/10.3389/fmats.2023.1125328, URL https://www.frontiersin.org/journals/materials/articles/10.3389/fmats.2023.1125328.

[2] Mangalgiri Prakash D. Composite materials for aerospace applications. Bull Mater Sci 1999;22(3):657–64. http://dx.doi.org/10.1007/BF02749982.

[3] Bajurko Piotr. Comparison of damage resistance of thermoplastic and thermoset carbon fibre-reinforced composites. J Thermoplast Compos Mater 2021;34(3):303–15. http://dx.doi.org/10.1177/0892705719844550.

[4] Alshammari Basheer A, Alsuhybani Mohammed S, Almushaikeh Alaa M, Alotaibi Bander M, Alenad Asma M, Alqahtani Naif B, Alharbi Abdullah G. Comprehensive review of the properties and modifications of carbon fiber-reinforced thermoplastic composites. Polym 2021;13(15). http://dx.doi.org/10.3390/polym13152474, URL https://www.mdpi.com/2073-4360/13/15/2474.

[5] Muzzy John D, Kays Ancil O. Thermoplastic vs. thermosetting structural composites. Polym Compos 1984;5(3):169–72. http://dx.doi.org/10.1002/pc.750050302, URL https://4spepublications.onlinelibrary.wiley.com/doi/abs/10.1002/pc.750050302.

[6] Sudhin Au, Remanan Manu, Ajeesh Gopinad, Jayanarayanan Karingamanna. Comparison of properties of carbon fiber reinforced thermoplastic and thermosetting composites for aerospace applications. Mater Today: Proc 2020;24:453–62. http://dx.doi.org/10.1016/j.matpr.2020.04.297, URL https://www.sciencedirect.com/science/article/pii/S2214785320329199, International Conference on Advances in Materials and Manufacturing Applications, IConAMMA 2018, 16th -18th August, 2018, India.

[7] Mahat Khairul B, Alarifi Ibrahim, Alharbi Abdulaziz, Asmatulu Ramazan. Effects of UV light on mechanical properties of carbon fiber reinforced PPS thermoplastic composites. Macromol Symp 2016;365(1):157–68. http://dx.doi.org/10.1002/masy.201650015, URL https://onlinelibrary.wiley.com/doi/10.1002/masy.201650015.

[8] Dong Shaoce, Zhou Ping, Ning Zhao, Wu Xu, Li Chenggao, Xian Guijun. Durability of carbon- and glass-fiber reinforced thermoplastic polymer composites: A literature review. J Build Eng 2024;98:111055. http://dx.doi.org/10.1016/j.jobe.2024.111055, URL https://www.sciencedirect.com/science/article/pii/S2352710224026238.

[9] Wang Wen-Jing, Dong Yuan, Wei Zhi-Mei, Long Sheng-Ru, Yang Jie, Yang Jia-Cao, Wang Xiao-Jun. Hydrothermal aging of short glass fiber reinforced polyphenylene sulfide composites and property prediction. Polym Degrad Stab 2023;217:110503. http://dx.doi.org/10.1016/j.polymdegradstab.2023.110503, URL https://linkinghub.elsevier.com/retrieve/pii/S0141391023002537.

[10] Wang Zike, Xian Guijun, Zhao Xiao-Ling. Effects of hydrothermal aging on carbon fibre/epoxy composites with different interfacial bonding strength. Constr Build Mater 2018;161:634–48. http://dx.doi.org/10.1016/j.conbuildmat.2017.11.171, URL https://linkinghub.elsevier.com/retrieve/pii/S0950061817323905.

[11] Zhuang Xiangjie, Ma Junsen, Dan Yi, Jiang Long, Huang Yun. Hydrothermal aging of carbon fiber reinforced epoxy composites with different interface structures. Polym Degrad Stab 2023;212:110352. http://dx.doi.org/10.1016/j.polymdegradstab.2023.110352, URL https://linkinghub.elsevier.com/retrieve/pii/S0141391023001040.

[12] Cysne Barbosa Ana P, P. Fulco Ana Paula, S.S. Guerra Erick, K. Arakaki Franscisco, Tosatto Márcio, B. Costa Maria Carolina, D. Melo José Daniel. Accelerated aging effects on carbon fiber/epoxy composites. Compos Part B: Eng 2017;110:298–306. http://dx.doi.org/10.1016/j.compositesb.2016.11.004, URL https://www.sciencedirect.com/science/article/pii/S1359836816313579.

[13] Deng Kelin, Luo Bin, Suo Haoyuan, Zhang Kaifu, Wang Linxuan, Cheng Hui, Liang Biao. Characterization of material degradation mechanism of carbon fiber reinforced epoxy resin composites under ultraviolet radiation and salt-fog synergistic environment. Polym Compos 2024;45(1):805–24. http://dx.doi.org/10.1002/pc.27816, URL https://4spepublications.onlinelibrary.wiley.com/doi/abs/10.1002/pc.27816.

[14] Meyer Daniel R, Carnevale Paola, Bersee Harald EN. PPSS: new thermoplastic for high performance composite applications. Plast Rubber Compos 2010;39(3–5):122–7. http://dx.doi.org/10.1179/174328910X12647080902330.

[15] Barile Marco, Lecce Leonardo, Iannone Michele, Pappadà Silvio, Roberti Pierluca. Thermoplastic composites for aerospace applications. In: Pantelakis Spiros, Tserpes Konstantinos, editors. Revolutionizing aircraft materials and processes. Cham: Springer International Publishing; 2020, p. 87–114. http://dx.doi.org/10.1007/978-3-030-35346-9_4.

[16] Patel Parina, Hull T Richard, Lyon Richard E, Stoliarov Stanislav I, Walters Richard N, Crowley Sean, Safronava Natallia. Investigation of the thermal decomposition and flammability of PEEK and its carbon and glass-fibre composites. Polym Degrad Stab 2011;96(1):12–22. http://dx.doi.org/10.1016/j.polymdegradstab.2010.11.009, URL https://www.sciencedirect.com/science/article/pii/S0141391010004167.

[17] Dolo Guillaume, Férec Julien, Cartié Denis, Grohens Yves, Ausias Gilles. Model for thermal degradation of carbon fiber filled poly(ether ether ketone). Polym Degrad Stab 2017;143:20–5. http://dx.doi.org/10.1016/j.polymdegradstab.2017.06.006, URL https://www.sciencedirect.com/science/article/pii/S0141391017301702.

[18] Rival Guilhem, Dantras Éric, Paulmier Thierry. Ageing of PEEK/Carbon fibre composite under electronic irradiations: Influence on mechanical behaviour and charge transport. Compos Part A: Appl Sci Manuf 2022;154:106769. http://dx.doi.org/10.1016/j.compositesa.2021.106769, URL https://www.sciencedirect.com/science/article/pii/S1359835X21004796.

[19] Mylläri Ville, Ruoko Tero-Petri, Järvelä Pentti. The effects of UV irradiation to polyetheretherketone fibres – Characterization by different techniques. Polym Degrad Stab 2014;109:278–84. http://dx.doi.org/10.1016/j.polymdegradstab.2014.08.003, URL https://www.sciencedirect.com/science/article/pii/S0141391014002936.

[20] Singh Baljit, Sharma Nisha. Mechanistic implications of plastic degradation. Polym Degrad Stab 2008;93(3):561–84. http://dx.doi.org/10.1016/j.polymdegradstab.2007.11.008, URL https://www.sciencedirect.com/science/article/pii/S0141391007003539.

[21] Niu Yi-Fan, Yang Ying, Li Tian-Yi, Yao Jia-Wei. Effects of UV irradiation and condensation on poly(ether-ether-ketone)/carbon fiber composites from nano- to macro-scale. High Perform Polym 2018;30(2):230–8. http://dx.doi.org/10.1177/0954008316689600.

[22] Batista Natassia L, Rezende Mirabel C, C.Botelho Edson. The influence of crystallinity on the weather resistance of CF/PEEK composites. Appl Compos Mater 2021;28(1):235–46. http://dx.doi.org/10.1007/s10443-020-09863-x.

[23] Batista Natassia L, Rezende Mirabel C, Botelho Edson C. Effect of crystallinity on CF/PPS performance under weather exposure: Moisture, salt fog and UV radiation. Polym Degrad Stab 2018;153:255–61. http://dx.doi.org/10.1016/j.polymdegradstab.2018.03.008, URL https://linkinghub.elsevier.com/retrieve/pii/S0141391018300776.

[24] Faria Maria CM De, Costa Michelle L, Oliveira Pedro C De, Botelho Edson C. The effect of the ocean water immersion and UV ageing on the dynamic mechanical properties of the PPS/glass fiber composites. J Reinf Plast Compos 2011;30(20):1729–37. http://dx.doi.org/10.1177/0731684411427483, URL http://journals.sagepub.com/doi/10.1177/0731684411427483.

[25] Quan Dong, Deegan Brian, Byrne Lorcán, Scarselli Gennaro, Ivanković Alojz, Murphy Neal. Rapid surface activation of carbon fibre reinforced PEEK and PPS composites by high-power UV-irradiation for the adhesive joining of dissimilar materials. Compos Part A: Appl Sci Manuf 2020;137:105976. http://dx.doi.org/10.1016/j.compositesa.2020.105976, URL https://linkinghub.elsevier.com/retrieve/pii/S1359835X20302153.

[26] Yilmaz Taner, Sinmazcelik Tamer. Effects of hydrothermal aging on glass–fiber/polyetherimide (PEI) composites. J Mater Sci 2010;45(2):399–404. http://dx.doi.org/10.1007/s10853-009-3954-1, URL http://link.springer.com/10.1007/s10853-009-3954-1.

[27] ASTM Standard G147-17. Standard practice for conditioning and handling of nonmetallic materials for natural and artificial weathering tests, URL http://www.astm.org/cgi-bin/resolver.cgi?D5229D5229M-14.
[28] ASTM Standard D4329-21. Standard Practice for Fluorescent Ultraviolet UV Lamp Apparatus Exposure of Plastics, URL https://www.astm.org/d4329-21.html.
[29] ASTM Standard D3039-17. Test method for tensile properties of polymer matrix composite materials, URL http://www.astm.org/cgi-bin/resolver.cgi?D3039D3039M-17.
[30] Gao Shang-Lin, Kim Jang-Kyo. Cooling rate influences in carbon fibre/PEEK composites. Part 1. Crystallinity and interface adhesion. Compos Part A: Appl Sci Manuf 2000;31(6):517–30. http://dx.doi.org/10.1016/S1359-835X(00)00009-9, URL https://www.sciencedirect.com/science/article/pii/S1359835X00000099.
[31] Courvoisier Emilie, Bicaba Yoann, Colin Xavier. Multi-scale and multi-technique analysis of the thermal degradation of poly(ether ether ketone). Polym Degrad Stab 2018;151:65–79. http://dx.doi.org/10.1016/j.polymdegradstab.2018.03.001, URL https://www.sciencedirect.com/science/article/pii/S0141391018300648.
[32] Arao Yoshihiko, Koyanagi Jun, Hatta Hiroshi, Kawada Hiroyuki. Analysis of time-dependent deformation of CFRP considering the anisotropy of moisture diffusion. Adv Compos Mater 2008;17(4):359–72. http://dx.doi.org/10.1163/156855108X385276, URL http://www.tandfonline.com/doi/abs/10.1163/156855108X385276.
[33] Pinlova Barbora, Nowack Bernd. From cracks to secondary microplastics - surface characterization of polyethylene terephthalate (PET) during weathering. Chemosphere 2024;352:141305. http://dx.doi.org/10.1016/j.chemosphere.2024.141305, URL https://www.sciencedirect.com/science/article/pii/S004565352400198X.
[34] Oshima Sota, Higuchi Ryo, Kato Masaya, Minakuchi Shu, Yokozeki Tomohiro, Aoki Takahira. Cooling rate-dependent mechanical properties of polyphenylene sulfide (PPS) and carbon fiber reinforced PPS (CF/PPS). Compos Part A: Appl Sci Manuf 2023;164:107250. http://dx.doi.org/10.1016/j.compositesa.2022.107250, URL https://www.sciencedirect.com/science/article/pii/S1359835X22004316.
[35] Zimmerman Dean A, Koenig Jack L, Ishida Hatsuo. Infrared spectroscopic analysis of poly(p-phenylene sulfide). Spectrochim Acta Part A: Mol Biomol Spectrosc 1995;51(13):2397–409. http://dx.doi.org/10.1016/0584-8539(95)01408-X, URL https://linkinghub.elsevier.com/retrieve/pii/058485399501408X.
[36] Hsiao Sheng-Huei, Yang Chin-Ping, Chen Yung-Chung, Wang Hui-Ming, Guo Wenjeng. Synthesis and properties of poly(ether imide)s derived from 2,5-bis (3,4-dicarboxy phenoxy) biphenyl dianhydride and aromatic ether–diamines. J Appl Polym Sci 2009;113(6):3993–4002. http://dx.doi.org/10.1002/app.30495, URL https://onlinelibrary.wiley.com/doi/10.1002/app.30495.
[37] Jean-Fulcrand Annelise, Masen Marc A, Bremner Tim, Wong Janet SS. Effect of temperature on tribological performance of polyetheretherketone-polybenzimidazole blend. Tribol Int 2019;129:5–15. http://dx.doi.org/10.1016/j.triboint.2018.08.001, URL https://www.sciencedirect.com/science/article/pii/S0301679X1830389X.
[38] Das Paritosh K, DesLauriers Paul J, Fahey Darryl R, Wood Frankie K, Cornforth Frederick J. Photodegradation and photostabilization of poly(p-phenylene sulfide). UV induced physicochemical changes. Polym Degrad Stab 1995;48(1):11–23. http://dx.doi.org/10.1016/0141-3910(95)00033-I, URL https://linkinghub.elsevier.com/retrieve/pii/014139109500033I.
[39] Fukui Kunihiro, Yamada Masaaki, Ichiba Genki, Prasetya Fandi Angga, Kuo Hsiu-Po, Huang An-Ni, Fukasawa Tomonori, Ishigami Toru. Effects of exposure temperature on degradation of polyphenylene sulfide non-woven bag-filter media by NO2 gas at high temperature. Adv Powder Technol 2023;34(10):104195. http://dx.doi.org/10.1016/j.apt.2023.104195, URL https://www.sciencedirect.com/science/article/pii/S0921883123002601.
[40] Gaitanelis Dimitrios, Worrall Chris, Kazilas Mihalis. Detecting, characterising and assessing PEEK's and CF-PEEK's thermal degradation in rapid high-temperature processing. Polym Degrad Stab 2022;204:110096. http://dx.doi.org/10.1016/j.polymdegradstab.2022.110096, URL https://www.sciencedirect.com/science/article/pii/S0141391022002749.
[41] Lee Youngchul, Porter Roger S. Crystallization of poly (etheretherketone)(PEEK) in carbon fiber composites. Polym Eng Sci 1986;26(9):633–9.
[42] Batista Natassia Lona, de Faria Maria Cândida Magalhães, Iha Koshun, de Oliveira Pedro Carlos, Botelho Edson Cocchieri. Influence of water immersion and ultraviolet weathering on mechanical and viscoelastic properties of polyphenylene sulfide–carbon fiber composites. J Thermoplast Compos Mater 2015;28(3):340–56. http://dx.doi.org/10.1177/0892705713484747.
[43] Ghanbari Lina N, Previte Joseph P, Wiggins Jeffrey S, McNair Olivia D. Thermal history dependent rheology, crystallization, and fusion joint strength of polyphenylene sulfide/carbon fiber thermoplastic composites. J Thermoplast Compos Mater 08927057251322156. http://dx.doi.org/10.1177/08927057251322156.
[44] Rodriguez Ana K, Mansoor Bilal, Ayoub Georges, Colin Xavier, Benzerga Amine A. Effect of UV-aging on the mechanical and fracture behavior of low density polyethylene. Polym Degrad Stab 2020;180:109185. http://dx.doi.org/10.1016/j.polymdegradstab.2020.109185, URL https://www.sciencedirect.com/science/article/pii/S0141391020301178.
[45] Fayolle Bruno, Richaud Emmanuel, Colin Xavier, Verdu Jacques. Review: degradation-induced embrittlement in semi-crystalline polymers having their amorphous phase in rubbery state. J Mater Sci 2008;43(22):6999–7012. http://dx.doi.org/10.1007/s10853-008-3005-3.
[46] Shi Zhongmeng, Zou Chao, Zhou Feiyu, Zhao Jianping. Analysis of the mechanical properties and damage mechanism of carbon fiber/epoxy composites under UV aging. Mater 2022;15(8):2919. http://dx.doi.org/10.3390/ma15082919, URL https://www.mdpi.com/1996-1944/15/8/2919.